ACS OMEGA

http://pubs.acs.org/journal/acsodf

Article

Synergetic Enhancement of Pb^{2+} and Zn^{2+} Adsorption onto Size-Selective Sludge Biochar Portions in Multiple Ion Solution Systems

Haoming Chen,[⊥] Yao Peng,[⊥] Lingyi Tang, Fangfang Min, Muhanmaitijiang Nazhafati, Chen Li, Jian Ge, Haihou Wang,* and Junji Li*

Cite This: *ACS Omega* 2022, 7, 496−503

Read Online

ACCESS | Metrics & More | Article Recommendations | Supporting Information

ABSTRACT: Particle size, one of the predominant factors that affect the adsorption capacity of biochar, has been widely investigated. However, correlative studies on a coexistence system containing various ions together with differentiated particle sizes are scarce. In this study, samples of municipal solid waste (sludge) biochar (SB) with different particle sizes were separated and examined for the adsorption performance in bi-cation (Pb^{2+}/Zn^{2+}) and multi-ion (Pb^{2+}, Zn^{2+} and Cl^-) systems. The results showed that the adsorption capacity is influenced by both particle size and ion configurations. The effective stabilization ability of a small size group can be attributed to the most non-bioavailable fraction. Meanwhile, the acidic soluble and non-bioavailable fraction of Pb^{2+}/Zn^{2+} reached more than 90%. The mixed adsorption experiment showed that Pb^{2+} would compete for the adsorption sites of biochar with Zn^{2+}, and Cl^- intervention could improve the adsorption of Pb^{2+} (2.33−6.93%) and Zn^{2+} (16.52−18.01%) on biochar. Further, X-ray diffraction spectra and phosphorus concentration dynamics and kinetics simulations revealed that more abundant active sites in the formatted pyromorphite were able to be exposed in the presence of Cl^-. The small-size portion of SB therefore exhibited excellent potential for the long-term heavy metal remediation under practical conditions of multi-ion systems in an actual environment.

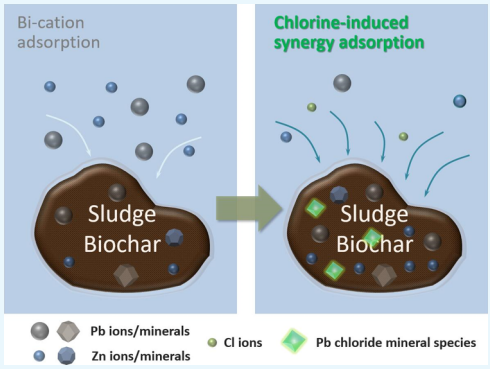

1. INTRODUCTION

Lead (Pb) is one of the most common contaminants in the environment with long-term persistence.[1] It is a cumulative pollutant, which lead to high toxicity, for example, impairing neurological development and interfering with functioning of enzymes.[2−4] About half a million deaths and over nine million disability-adjusted life years were attributed to Pb exposure in 2016.[5] Geogenic and anthropogenic sources are the main causes of Pb pollution, such as mining, batteries, and smelting operations, all related to human activities. It is noteworthy that the subsequent occurring of pollution in water and soil environment is more common and dangerous. For example, it is easy for the toxic metal ions of acid mine drainage to enter the food chain via surface runoff and soil diffusion, which impose risks on human beings and aquatic life.[6,7] Therefore, to solve these problems, efficient remediation materials are imperative for solidification and stabilization of heavy metals.

Biochar is a promising carbon-based remediation material, produced by heating biological residues with limited air supply.[8] Applying biochar in water treatment or soil remediation to immobilize heavy metals and reduce environmental risks is now regarded as a green sustainable remediation technology.[9,10] Biochar reduces the bioavailability/mobility of heavy metals through various mechanisms, for example, physical adsorption, cation exchange, electrostatic interaction, precipitation, and complexation.[11,12] Among them, (1) the heavy metals adsorbed on biochar via physical adsorption and cation exchange comprise the bioavailable fraction with direct risks to plants and humans; (2) those adsorbed through cation−π interaction are the potentially bioavailable fraction; and (3) those through surface complexation represent the non-bioavailable fraction. The non-bioavailable components can maintain good stability under environmental alteration. Therefore, it is critical to reduce the bioavailability of heavy metal pollutants when applying biochar in remediation.[13]

Mixed ion systems and biochar particle size are common factors of priority in heavy metals remediation. Previous studies have demonstrated that a decrease in particle size of biochar can improve adsorption capacity of heavy metals due to higher surface area.[14] Moreover, particle size also influences adsorption capacity by limiting diffusion penetration depth. Micromilling increases the surface area, thus enhances adsorption capacity until particle radius is smaller than the

Received: September 6, 2021
Accepted: December 10, 2021
Published: December 27, 2021

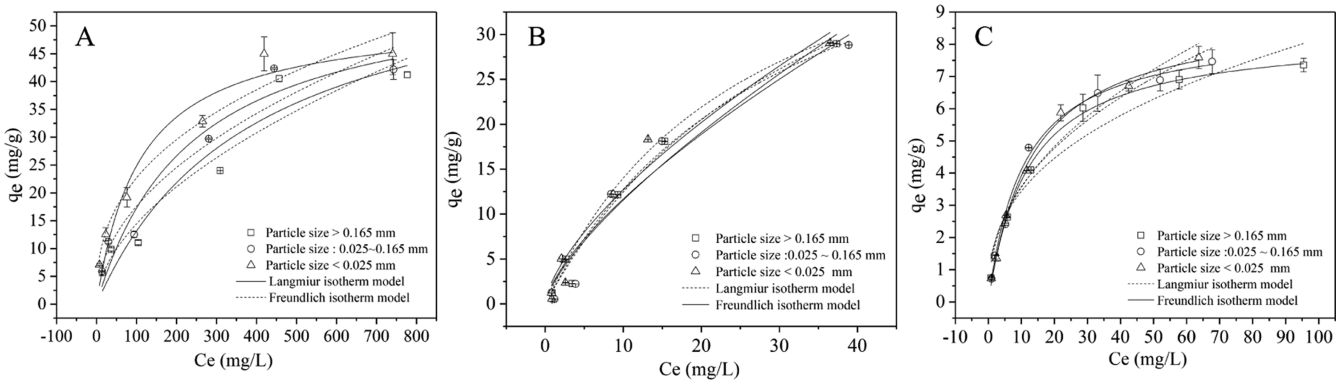

Figure 1. Adsorption isotherms for Pb (A), Zn (B) and Zn with Cl^- (C) onto the three types of biochar in the batch experiment (S1: >0.165, S2: 0.025−0.165, S3: <0.025 mm).

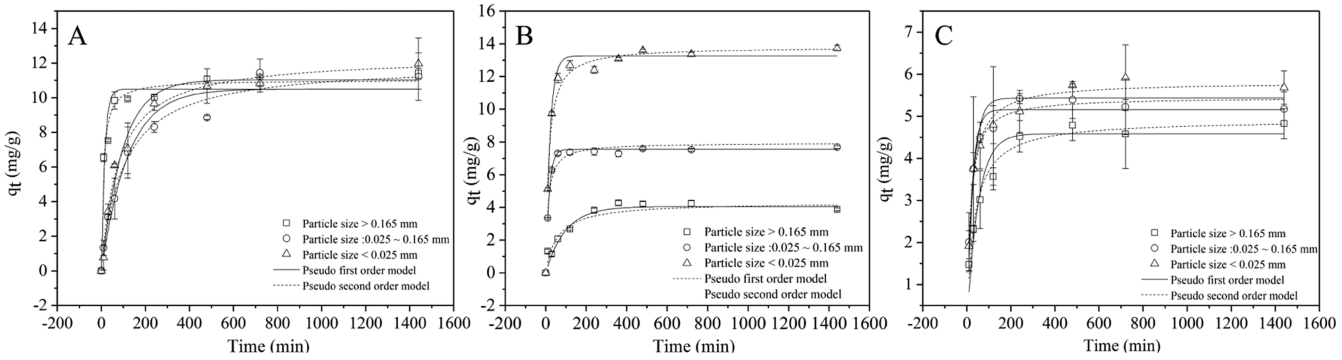

Figure 2. Adsorption kinetics for Pb (A), Zn (B) and Zn with Cl^- (C) onto three types of biochar in the batch experiment (S1: >0.165, S2: 0.025−0.165, S3: <0.025 mm).

diffusion penetration depth.[15] Heavy metal adsorption could be restricted by competitive behavior of the involved metals for biochar sorption sites.[16] Some study showed that comparing to monometal solutions, the adsorption capacity of biochar is usually lower in mixed solutions.[16−18] Among the common heavy metals (Pb, Cd, Cr, Cu, Zn), biochar has the highest adsorption capacity of Pb^{2+}, while Zn^{2+} is one of the most affected metal ions in multi-metal systems.[16] Hence, Pb^{2+} and Zn^{2+} are typical metal ions in mixed adsorption experiments. Additionally, the presence of some ubiquitous anions may also promote the removal of heavy metals. For example, $ZnCl_2$ (Cl^-) is commonly used in the preparation and modification of carbon or other materials to improve absorption capacity of Pb^{2+}.[19−22] Although several studies have estimated mixed sorption of heavy metals by biochar, few research studies focused on the synergistic effects considering both particle size and chlorine anion in multi-metal adsorption. In addition, the mixed adsorption behavior of Pb and Zn on some specific biochars is not clear. At the same time, as one of the most common anions in the environment, Cl^- plays an important synergistic role in promoting the mineralization of heavy metals (especially for Pb: pyromorphite). Therefore, it is important to study the mixed adsorption mechanism of Pb and Zn in the presence of Cl^- on biochars with different particle sizes, which would help evaluate the risky state modification of Pb adsorbed on biochars in real aquatic and soil environment.

This study investigated the adsorption behavior of Pb^{2+} onto biochar with different particle sizes and the influence of competition of other ions. We hypothesized that the presence of Zn^{2+} and Cl^- would increase the adsorption of lead onto biochar by some certain mechanism. Accordingly, the concentration variations of soluble P, Pb^{2+}, and Zn^{2+} were analyzed by inductively coupled plasma optic emission spectrometry (ICP−OES), and meanwhile, the formation and mineralogy of the generated minerals on biochar during Pb^{2+} and Zn^{2+} mineralization were investigated by X-ray diffraction (XRD), scanning electron microscopy (SEM), and sequential extraction tests.

2. RESULTS

2.1. Adsorption Isotherms in Bi-Cation System.

Experimental data were fitted by the Langmuir and Freundlich isotherm models after Pb^{2+} batch adsorption studies. The nonlinear forms of the two models were used in this study. The results are shown in Figure 1. Generally, to find out the best fitting isotherm model, the obtained correlation coefficient (R^2) values are compared with each other. It showed that the adsorption isotherm of Pb^{2+} could be identified using both models because R^2 values were close with each other (Table S1). The maximum adsorption capacities (Q_{max}) of Pb^{2+} in the Langmuir model were close to each other (~60 mg/g) considering the fitting errors. However, there was a subtle tendency that Q_{max} was in reverse to particle size. The constants that related to binding energy of S1, S2, and S3 were 0.003, 0.004, and 0.009 L/mg, respectively, indicating the highest binding energy of S3. The Freundlich model seemed to describe adsorption better because of higher R^2. K_f is a constant related to the sorption capacity, and $1/n$ is an empirical parameter related to the intensity of sorption, which varies with the heterogeneity of the material. It was inferred that K_f increased with decreasing particle size.

https://doi.org/10.1021/acsomega.1c04901
ACS Omega 2022, 7, 496−503

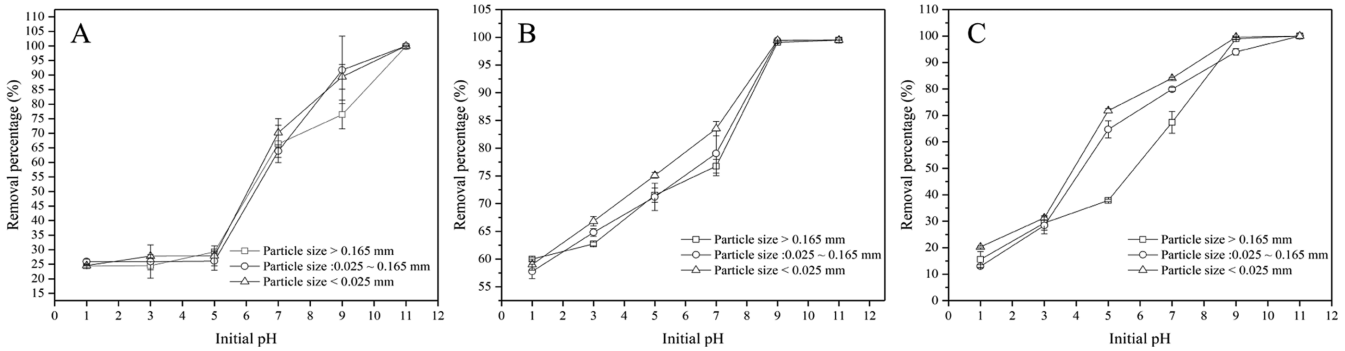

Figure 3. Removal percentage of Pb^{2+} (A), Zn^{2+} (B) and Zn^{2+} with Cl^{-} (C) by three types of biochar in the bi-cation solution with various initial pH values (S1: >0.165, S2: 0.025−0.165, S3: <0.025 mm).

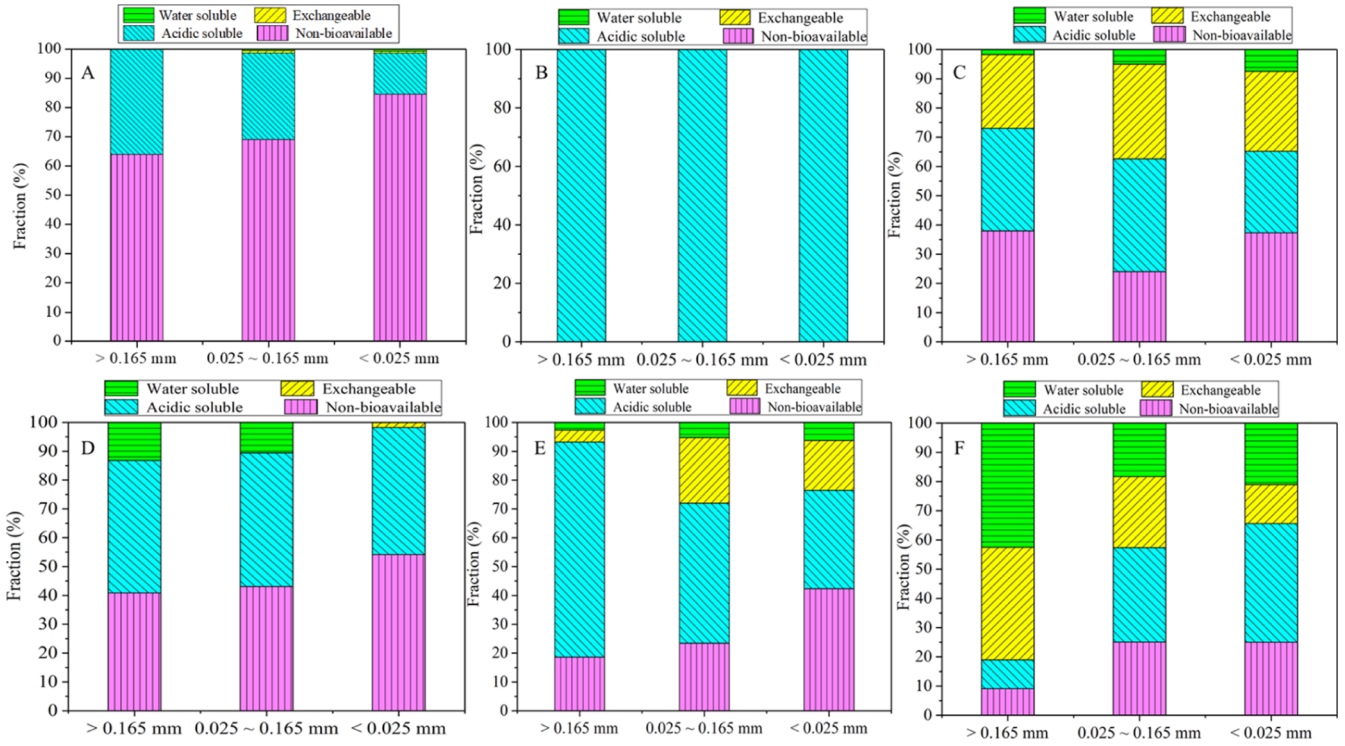

Figure 4. $Pb^{2+}$and Zn^{2+} fractions (%) in mono-metal cation, bi-cation and multi ion system after 24 h adsorption onto biochar. Mono-metal cation: (A) Pb^{2+} fractions, (B) Zn^{2+} fractions, (C) Zn^{2+} fractions with Cl^{-}; bi-cation system: (D) Pb^{2+} fractions, Zn^{2+} is not fixed by biochar in the bi-cation system; multi ion system: (E) Pb^{2+} fractions, (F) Zn^{2+} fractions (S1: >0.165, S2: 0.025−0.165, S3: <0.025 mm).

In contrast, the Langmuir model was well applied in Zn^{2+} adsorption because R^2 values were beyond 0.99 for all of the three types of biochar, while R^2 values of Freundlich were ∼0.96, which suggested a monolayer adsorption of Zn^{2+}. The Q_{max} of Zn^{2+} in the Langmuir model was 8.3, 8.5, and 9.03 mg/g for S1, S2, and S3, respectively (Table S1), indicating more adsorption capacity of Zn^{2+} for biochar with smaller size. The b values were close to each other among the three types of biochar, which were ∼0.08 L/mg. To clarify the adsorption mechanism, the specific surface area of S1, S2, and S3 were tested, which equaled 24.04, 30.48, and 32.62 m^2/g, respectively (Table S2).

2.2. Adsorption Kinetics and Phosphorus Dynamics in a Bi-Cation System. The pseudo-first-order kinetic model and pseudo-second-order kinetic model were utilized to estimate the mechanism involved in the adsorption process of Pb^{2+} and Zn^{2+} onto SB (Figure 2). The R^2 values of the pseudo-second-order kinetic model were higher than those of pseudo-first-order model (Table S3), which suggested that a pseudo-second-order model could better describe the adsorption processes of Pb^{2+} and Zn^{2+}, indicating a chemisorption dominated the adsorption.[23]

An intraparticle diffusion model was applied to further investigate the adsorption kinetics. It shows that decrease in particle size could promote all film diffusion rates (slope 1) and nearly all pore diffusion rates (the last slope). Smaller particle size also decreased the boundary layer's thickness (intercept 1) (Figure S6). According to previous interpretations,[23,24] film diffusion dominated the adsorption rates in the study, as slope 1 was much higher that other slopes in each treatment. From Figure S6G−I, stage 2, corresponding to adsorption on the biochar surface with physical or chemical binding, could be distinguished and its slope increased, which can be attributed to more available functional groups with the extending surface area.

https://doi.org/10.1021/acsomega.1c04901
ACS Omega 2022, 7, 496−503

Concentrations of phosphorus in the adsorption kinetics were also detected. Soluble P from S1 in the experiment of Pb^{2+}/Zn^{2+} adsorption kinetics in the bi-cation system was higher than that from S2 and S3 (Figure S1), which also occurred in the multi-ion system when equilibrium was attained (Figure S2). Soluble P from S1 fluctuated with a maximum at ~500 min (11.79 mg/L) while soluble P from S2 and S3 culminated at ~700 min (10.77 and 10.73 mg/L, respectively) in the adsorption kinetics of Pb. In the adsorption kinetics of Zn, soluble P peaked at ~500 min with a much higher value (20.94, 16.69, and 16.46 mg/L, respectively).

2.3. Effects of Initial pH on Adsorption of $Pb^{2+}$and Zn^{2+}. The adsorbed Pb^{2+} at initial pH values of 2−5 was relatively low for S1, S2, and S3 (24.4−27.89%) (Figure 3). Acidic condition inhibited the formation of Pb minerals, for example, cerussite ($PbCO_3$), lead hydroxide [$Pb(OH)_2$], and pyromorphite [$Pb_5(PO_3)_3Cl$] or hydroxypyromorphite [$Pb_5(PO_3)_3OH$].[25] After initial pH of 5, Pb^{2+} removal percentage rapidly rose with increasing initial pH due to the enhanced deprotonation process on SB surface and more negative sites.[26] Soluble Pb^{2+} was removed absolutely at initial pH of 11 (100%). The percentages of Pb^{2+} removed by S1, S2, and S3 were close at each initial pH values.

Differing from Pb^{2+}, the adsorbed Zn^{2+} gradually increased when initial pH value increased, and differentiation between biochar with different particle sizes at initial pH values of 4−9. S3 adsorbed more Zn^{2+} than S2 and followed by S1 at initial pH values of 5. Response of Pb^{2+} adsorption to pH values differed from that of Zn adsorption mainly due to cation properties.

2.4. Sequential Extraction Results. The stability of Pb^{2+} and Zn^{2+} on each biochar determined by sequential extraction tests is shown in Figure 4. In the mono-metal system of Pb^{2+}, the majority of adsorbed Pb^{2+} on S1 (64.02%), S2 (69.12%), and S3 (84.63%) were in the non-bioavailable fraction, corresponding to the decreasing particle size. Acidic soluble fraction decreased from 35.87 to 14.10% when particle became finer. The exchangeable fraction and water soluble fraction were so low (below 1%) that could be negligible.

The acidic soluble fraction of Zn^{2+} was the dominant phase (Figure 4B). However, when incorporated Cl^- into the solution (Figure 4C), the non-bioavailable fractions of Zn^{2+} were 37.96, 24.00, and 37.34% for S1, S2, and S3, respectively. The acidic soluble fraction of Zn^{2+} was 35.06 and 38.63% for S1 and S2, and followed by S3 (27.90%).

Compared with single-cation adsorption, adsorption capacities of both Pb^{2+} and Zn^{2+} were promoted in a bi-cation adsorption system (Table 1). For Pb^{2+}, the ratios of non-bioavailable fractions gave the way to others, while Zn^{2+} was excluded from adsorption, resulting that each fraction was under detection limits. In a multi-ion system, adsorption capacities of Zn^{2+} for S1, S2, and S3 increased by 18.01, 16.52, and 17.64%, respectively, while adsorption capacities of Pb^{2+} for S1, S2, and S3 were slightly altered (only 4.54, 6.93, and 2.33%) of those in the bi-cation system. Non-bioavailable fractions of Pb^{2+} and Zn^{2+} decreased in the multi-ion system. The non-bioavailable fractions of Pb^{2+} for S1, S2, and S3 were 18.62, 23.47, and 42.35% respectively, which increased with decreasing particle size of SB. This tendency also occurred in Zn^{2+} (9.14, 25.04, and 25.03% for S1, S2, and S3). The results interpreted that fine-sized SB had a smaller environmental risk than others.

Table 1. Adsorption Capacity of Pb^{2+} and Zn^{2+} in the Bi-Cation and Multi-Ion System (S1: >0.165, S2: 0.025−0.165, S3: <0.025 mm)[a]

		adsorption capacity (mg/g)		
	type of biochar	single-cation	bi-cation	multi-ion
Pb^{2+}	particle size >0.165 mm	11.416	19.721	20.616
	particle size: 0.025−0.165 mm	11.215	24.966	26.695
	particle size <0.025 mm	11.974	29.018	26.694
Zn^{2+}	particle size >0.165 mm	6.526 (12.152)	0.01	18.235
	particle size: 0.025−0.165 mm	6.482 (12.237)	0.006	18.067
	particle size <0.025 mm	7.172 (12.211)	0.37	18.600

[a]The bracketed data is the data of $Zn(NO_3)_2$.

2.5. XRD Results. The XRD patterns of the three types of SB after adsorption of both Pb^{2+} and Zn^{2+} with existence of Cl^- are shown in Figure 5. The peaks at 17.8°, 24.8°, 25.5°, 43.5° and the peaks at 11.1°, 20.1°, 27.1°, 34.2°confirmed the primarily existence of $PbCO_3$ and hydrocerussite [$Pb_3(CO_3)_2(OH)_2$] on biochar (Figures 5 and S3).[27] The peaks at 13.8°, 22.5°, 34.7°, 43°, and 45.8°were attributed to $ZnCO_3$ and peaks at 19.3°, 29°, 39.5°, and 48.2° represented $Zn_3(PO4)_2$. $Zn(OH)_2$ was observed according to peaks at 24.9° and 27.1° (Figures 5 and S4).

In the multi-ion system, formation of $Pb_5(PO_3)_3Cl$ was confirmed due to new peaks at 20.5°, 35.9° and enhanced intensity of peaks at 26.2° in Figure 5B,C, and $Pb_3(PO_3)_2(OH)_2$ corresponding to the new peak at 21.8°.[28,29] In addition, compared with XRD patterns in the bi-cation system (Figures S3 and S4), weakened noise in Figure 5 indicated enhanced mineralization of Pb and Zn in the multi-ion system.

3. DISCUSSION

In this paper, the adsorption of lead by SB and the co-adsorption of lead and zinc with coexistence of Cl^- were studied. The particle size of SB has a great influence on the adsorption capacity which should be ascribed to the compositional difference, and physical properties such as specific surface area or the inner-pore structures.

Previous studies have shown that the coexistence of lead and zinc leads to the reduction of their adsorption capacity.[16,18] However, after introducing chloride ions into this study, it was found that the presence of Cl^- would increase the adsorption capacity of two heavy metals possibly via enhancement of forming Pb minerals. In the presence of Cl^-, the increase of Pb^{2+} adsorption capacity (2.33−6.93%) on biochar was lower than that of Zn^{2+} (16.52−18.01%), but the proportion of non-bioavailable Pb^{2+} (64.02−84.63%) was higher than that of Zn^{2+} (1.70−7.47%). In addition, sequential extraction results interpreted that the fine-sized biochar has a lower environmental risk and sustainability due to its low bioavailable portions (Figure 4, Table S5).

Influence of particle size on efficiency of heavy metal immobilization by biochar have been demonstrated.[30−32] The sorption capacity of biochar can be affected by particle size via the surface area and diffusion depth. The adsorption capacity of Pb^{2+}/Zn^{2+} for S3 was higher than that for S1 in this study, which mainly due to the increase of surface area caused by the decrease of particle size,[14] and it was confirmed by the

https://doi.org/10.1021/acsomega.1c04901
ACS Omega 2022, 7, 496−503

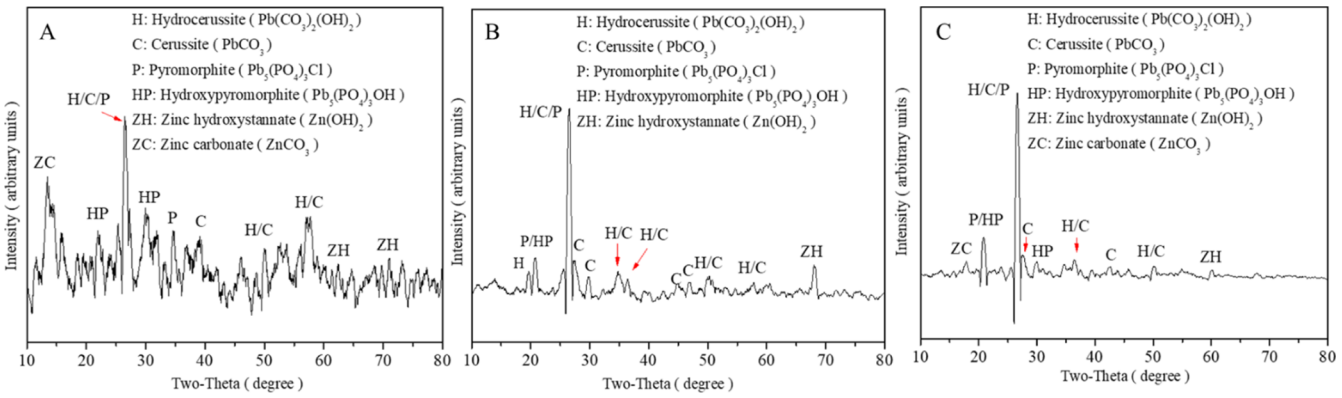

Figure 5. XRD patterns of each type of biochar after adsorption of $Pb^{2+}$and Zn^{2+} with existence of Cl^-. (A) Biochar with particle size >0.165 mm, (B) biochar with particle size 0.025−0.165 mm, (C) biochar with particle size <0.025 mm.

Brunauer−Emmett−Teller (BET) surface areas of biochar (Table S2). The reduction of particle size can not only increase the specific surface area of biochar but also improve its functional groups. ATR-IR results showed that the functional groups of small particle biochar are more abundant than those of large and medium particle biochar (Figure S5), which may be due to the increased surface area of biochar, resulting in more functional group exposure. Rich functional groups can significantly promote the adsorption of heavy metals by biochar,[33−35] which is also one of the reasons for the best adsorption effect of the smallest particle size. Previous studies have also confirmed that small particle size biochar had the most oxygen-containing functional groups, CEC, and negative charges as measured by the zeta potential, which improves the adsorption capacity of biochar for single heavy metals.[33] The shell adsorption model suggests that adsorbates are adsorbed on the exterior particle because of limited diffusion depth.[36] Therefore, the enhancing adsorption capacity of finer particle possibly results from more available and deeper reaction sites, which was coherent with the results of an intraparticle diffusion model. In addition, it was revealed that soluble P from S3 was lower than those from S2 and S1, which indicated that fine-sized SB had provided more sites for mineralization of phosphate.

The adsorption capacity of Pb^{2+} for SB was higher than that of Zn^{2+}, which is attributed to differences in chemical characteristics between them. Pb^{2+} has a smaller hydrated radius (4.01 Å) than that of Zn^{2+} (4.30 Å). Thus, Pb^{2+} is with a greater affinity for most functional groups in the organic matter. The higher electronegativity (2.33 for Pb and 1.65 for Zn) results in more favorably surface complexation or sorption of Pb.[16] Moreover, the solubility product constant (K_{sp}) of lead phosphate is also higher than that of zinc phosphate. All above lead to more adsorbed Pb on SB. However, the lower pK_H (negative log of hydrolysis constant) of Pb contributed to a lower slope of the removal curve before pH = 5 in pH treatment.

Involvement of anions is one of the important factors affecting mineral precipitation. It has been demonstrated that Cl^- could promotes the transformation of Pb minerals to Pb even though soluble P was ~10^{-12} mM.[25] A Pb/P mole ratio of $Pb_5(PO_3)_3Cl$ is higher than that of $Pb_3(PO_4)_2$. Moreover, increasing ion strength could improve solving of P from phosphate.[37] Hence, more Pb was precipitated by more "available P" provided in the multi-ion system to precipitate in the presence of Cl^-. So was Zn. In addition, the precipitation of Pb in solution can make the number of free spots on the biochar increase, which was beneficial to the adsorption of Zn on the biochar.

Stability and sustainability are two essential evaluation indices in heavy metal remediation via biochar in the environment. The heavy metals precipitate on biochar that can be dissolved in sodium acetate or acetic acid are considered as potentially bioavailable while the rest is considered as non-bioavailable.[13] Through sequential extraction, it was proved that compared with the bi-cation system, the components of heavy metal adsorption by three types of biochar with different particle sizes were significantly changed in the multi-ion system. The percentage of non-bioavailable fraction of Pb adsorbed on SB decreased when involving Zn^{2+} and Cl^-. However, adsorption capacity of Pb^{2+} for SB were increased, especially for fine-sized SB (S3) increased ~300%. Thus, the amount of non-bioavailable Pb^{2+} on fine-sized SB was much higher than that in the bi-cation system. This also indicates that pyromorphite may belong to non-bioavailable fraction in sequential extraction, which is consistent with the apparent increase of the peaks of XRD (Pb-mineral) in multi-ion systems. Non-bioavailable Pb and Zn will be released under strong acid conditions, but it rarely occurs in natural water. Hence, the non-bioavailable heavy metals formed by biochar adsorption are rather stable. Furthermore, P and Cl^- can significantly promote the adsorption and solidification of heavy metals (Pb and Zn) and can reduce the risk of re-decomposition of heavy metals. Especially in the soil environment, P and Cl^- exist widely, so they are easier to participate in the later maintenance of biochar remediation, so as to avoid secondary pollution.

4. CONCLUSIONS

In this study, the adsorption of Pb^{2+} and Zn^{2+} by biochars with different particle sizes was quantitatively analyzed. In the case of adsorption in the bi-cation system, the percentage of non-bioavailable fraction of Pb^{2+} was significantly higher than that of Zn^{2+}. In the multi-ion system, although the percentage of non-bioavailable fraction of Pb^{2+} on S3 decreased, its absolute quantity greatly increased due to increasing adsorption capacity. The presence of Cl^- promotes the formation of more stable Pb minerals, and other anions in the environment may also cooperate with Pb^{2+} to promote the precipitation on the surface of biochar. Therefore, under the condition of multiple-ion systems in the actual environment, fine-sized SB is

https://doi.org/10.1021/acsomega.1c04901
ACS Omega 2022, 7, 496−503

more conducive to the long-term stability for environmental treatment of heavy metal pollution.

5. MATERIALS AND METHODS

5.1. Material Preparation. A type of slight acidic biochar (SB, pH 6.36) was provided by Mississippi International Water (China) Ltd. The production details, and properties, have been well described in our previous studies.[38,39] SB was prepared from sludge (water content 80 wt %) at 600 °C, with BET surface area (13.62 m^2/g), average pore width (1.63 nm), total pore volume (0.081 cm^3/g), cation exchange capacity (40.43 cmol/kg), total N (1.66%), and total K (0.27%). SB was P-rich (1.71 wt %), which helps Pb-mineral formation.[27]

SB was dried at 105 °C for 24 h and sieved through 100 and 500 mesh, respectively. As a consequence, three particle sizes of SB were produced (>0.150, 0.025−0.150, and <0.025 mm). For simplicity, they were named S1, S2, and S3 to represent coarse-sized, moderate-sized, and fine-sized biochar, respectively, in this study. These samples were stored for the following analyses and experiments. The BET surface areas of them were characterized.

Pb^{2+} solution was prepared via $PbNO_3$ and Zn^{2+} solution was prepared by $ZnNO_3$. Thus, a solution with sole Pb^{2+} or Zn^{2+} was named the bi-cation system and coexistence of Pb, Zn, and Cl occurred in the mixture solution was named the muti-ion system.

5.2. Adsorption Experiments. Batch sorption experiments were conducted in polyethylene tubes in a temperature-controlled shaker (20 ± 1 °C). Solutions of 0.1 M HNO_3 and 0.1 M NaOH were used to adjust the pH of solutions when necessary. All solutions were adjusted to contain 0.01 M $NaNO_3$ to control the ion strength. To study the kinetics of adsorption onto biochar, 20 mL solutions with 1 mM Pb^{2+} or Zn^{2+} (pH = 5) were prepared and 0.1 g of biochar was added. The mixture was shaken at 200 rpm for a pre-determined time before filtration using a 0.22 μm filter. Shaking times were set at 5 min, 10 min, 20 min, 30 min, 1 h, 2 h, 3 h, 6 h, 12 h, 18 h, and 24 h for kinetics study. For the adsorption equilibrium study, 0.1 g of biochar was added to 20 mL solutions (pH = 5) containing different metal concentrations (0.1, 0.2, 0.4, 0.8, 2, 3, and 5 mM). Then, after shaking for 24 h, the mixtures were centrifuged at 4000 rpm for 2 min. The supernatants were filtered and the concentrations of metal ions were determined. The precipitates were dried at 60 °C for XRD analysis. All the three types of SB underwent the same treatment described above.

To estimate the effects of pH on adsorption of heavy metals, the three types of SB were added in 20 mL solutions with 1 mM metals, respectively. 1 M HNO_3 and 1 M NaOH were applied to adjust pH values of solutions to 1.0, 3.0, 5.0, 7.0, 9.0, and 11.0. They were shaken at 200 rpm for 24 h and then filtered for analysis.

Mixed adsorption between Pb^{2+} and Zn^{2+} was conducted in the bi-cation solution containing 1 mM Pb^{2+} and 2 mM Zn^{2+} and in the multi-ion solution, with 4 mM Cl^-. 0.1 g of S1, S2, and S3 were added in the multi-metal solution, respectively. Hence, the effect of particle size was also considered. After shaking at 200 rpm for 24 h, the suspensions were centrifuged and collected. The metal ions in the supernatant were then determined and the precipitate was further analyzed in sequential extraction described in the following sentences.

The modified sequential extraction has been used to distinguish various fractions of metals in previous studies.[13] This method is widely recognized, especially in the joint study of biochar. Hence, the precipitates in the mixed adsorption experiment, and those obtained in adsorption kinetics at the same dosage of each metal, were analyzed through the modified sequential extraction. According to Shen et al.'s research,[13] the four extraction steps correspond to four heavy metal forms in turn: ① water soluble fraction: the 0.1 g solid residue (after reaction) was mixed with 20 mL deionized water and shaken for 24 h; ② exchangeable fraction: the solid residue from ① was extracted with 8 mL of 0.5 M $MgCl_2$ (adjusted to pH 7.0 using NaOH or HCl) and shaken for 20 min; ③ acidic soluble fraction: the solid residue from ② was extracted with 8 mL of 1 M NaOAc (adjusted to pH 5.0 with HOAc) and shaken for 5 h at room temperature; ④ non-bioavailable fraction: the solid residue from ③ was digested with 9 mL of 36% HCl and 3 mL of 70% HNO_3 for 16 h, then heated at 95 °C for 2 h. All reactions were carried out at room temperature and details are shown in Supporting Information.

5.3. Instrument. The formed minerals before and after the adsorption on to biochar were examined by XRD using a Bruker D8 diffractometer (Cu Kα; λ = 1.540 60 Å; 40 kV; 40 mA; and scanned from 5° to 65° at a speed of 0.02°/s). ATR-TR, a Nicolet iS5 Fourier-transform infrared spectrometer (Thermo Fisher Scientific Inc., Madison, USA), was used for spectra of the biochars. For a better visualization, asymmetric least squares fitting was conduct to subtract baselines ($\lambda = 10^6$ and P = 0.001). The concentrations of lead and zinc were analyzed by ICP-OES (Agilent 710). A calibration curve (1, 2.5, 5, 10, 25, and 50 mg/L) was prepared as the lead standard. The R^2 value of the internal standard curve was 0.999.

5.4. Statistical Analysis. All adsorption experiments were conducted in triplicates. Means and standard deviations were calculated for each treatment. Adsorption isotherms were determined using the Langmuir and Freundlich non-linear models. Adsorption kinetics were fitted via pseudo first-order, second-order kinetic, and intraparticle diffusion models. The curve fitting was conducted by Origin Pro and spreadsheet offered by Gihan.[40] The equations of models were referred to Shen.[41]

■ ASSOCIATED CONTENT

Supporting Information

The Supporting Information is available free of charge at https://pubs.acs.org/doi/10.1021/acsomega.1c04901.

Adsorption isotherm, structural parameters, adsorption kinetics, immobilization efficiency, soluble P content in bi-cation and multi-ion systems, and XRD patterns after mono-adsorption of Pb^{2+} and Zn^{2+} (PDF)

■ AUTHOR INFORMATION

Corresponding Authors

Haihou Wang − *Taihu Research Institute of Agricultural Sciences, Suzhou 215100 Jiangsu, China*; Phone: +86(512) 13912792290; Email: wanghaihou@126.com

Junji Li − *School of Environmental and Biological Engineering, Nanjing University of Science and Technology, Nanjing 210094, China*; orcid.org/0000-0002-3104-6824; Phone: +86(25) 15950507768; Email: junjili@njust.edu.cn

https://doi.org/10.1021/acsomega.1c04901
ACS Omega 2022, 7, 496−503

Authors

Haoming Chen − *School of Environmental and Biological Engineering, Nanjing University of Science and Technology, Nanjing 210094, China; College of Resources and Environmental Sciences, Nanjing Agricultural University, Nanjing, Jiangsu 210095, China*

Yao Peng − *China Design Group Environmental Technology Co., Ltd, Nanjing 210008, China*

Lingyi Tang − *College of Resources and Environmental Sciences, Nanjing Agricultural University, Nanjing, Jiangsu 210095, China*

Fangfang Min − *School of Environmental and Biological Engineering, Nanjing University of Science and Technology, Nanjing 210094, China*

Muhanmaitijiang Nazhafati − *School of Environmental and Biological Engineering, Nanjing University of Science and Technology, Nanjing 210094, China*

Chen Li − *School of Environmental and Biological Engineering, Nanjing University of Science and Technology, Nanjing 210094, China*

Jian Ge − *School of Environmental and Biological Engineering, Nanjing University of Science and Technology, Nanjing 210094, China*

Complete contact information is available at: https://pubs.acs.org/10.1021/acsomega.1c04901

Author Contributions

[⊥]H.C. and Y.P. contributed equally in this work.

Notes

The authors declare no competing financial interest.

■ ACKNOWLEDGMENTS

This work was supported by Natural Science Foundation of China project (nos. 42007105 and 62001224), Natural Science Foundation of Jiangsu Province (BK20190457 and BK20181165) and the 5th Scientific Research Project of "333 High-level Talents Training Project" of Jiangsu Province (BRA2020128), Scientific Research Funds of Nanjing University of Technology (AZ89991/197).

■ REFERENCES

(1) O'Connor, D.; Hou, D.; Ye, J.; Zhang, Y.; Ok, Y. S.; Song, Y.; Coulon, F.; Peng, T.; Tian, L. Lead-based paint remains a major public health concern: A critical review of global production, trade, use, exposure, health risk, and implications. *Environ. Int.* **2018**, *121*, 85−101.

(2) Naik, M. M.; Khanolkar, D.; Dubey, S. K. Lead-resistant Providencia alcalifaciens strain 2EA bioprecipitates Pb+2 as lead phosphate. *Lett. Appl. Microbiol.* **2013**, *56*, 99−104.

(3) Ma, L. Q.; Rao, G. N. Aqueous Pb reduction in Pb-contaminated soils by Florida phosphate rocks. *Water Air Soil Pollut.* **1999**, *110*, 1−16.

(4) Hou, D.; Qi, S.; Zhao, B.; Rigby, M.; O'Connor, D. Incorporating life cycle assessment with health risk assessment to select the "greenest" cleanup level for Pb contaminated soil. *J. Clean. Prod.* **2017**, *162*, 1157−1168.

(5) WHO. *Lead Poisoning and Health*, 2017.

(6) Lu, H.; Zhang, W.; Yang, Y.; Huang, X.; Wang, S.; Qiu, R. Relative distribution of Pb2+ sorption mechanisms by sludge-derived biochar. *Water Res.* **2012**, *46*, 854−862.

(7) Cheng, S.; Jang, J.-H.; Dempsey, B. A.; Logan, B. E. Efficient recovery of nano-sized iron oxide particles from synthetic acid-mine drainage (AMD) water using fuel cell technologies. *Water Res.* **2011**, *45*, 303−307.

(8) Shen, Z.; Hou, D.; Zhao, B.; Xu, W.; Ok, Y. S.; Bolan, N. S.; Alessi, D. S. Stability of heavy metals in soil washing residue with and without biochar addition under accelerated ageing. *Sci. Total Environ.* **2018**, *619−620*, 185−193.

(9) Lehmann, J.; Gaunt, J.; Rondon, M. Bio-char Sequestration in Terrestrial Ecosystems − A Review. *Mitig. Adapt. Strategies Glob. Change* **2006**, *11*, 395−419.

(10) Shen, Z.; Som, A. M.; Wang, F.; Jin, F.; McMillan, O.; Al-Tabbaa, A. Long-term impact of biochar on the immobilisation of nickel (II) and zinc (II) and the revegetation of a contaminated site. *Sci. Total Environ.* **2016**, *542*, 771−776.

(11) Cao, X.; Ma, L.; Gao, B.; Harris, W. Dairy-Manure Derived Biochar Effectively Sorbs Lead and Atrazine. *Environ. Sci. Technol.* **2009**, *43*, 3285−3291.

(12) Yang, X.; Wan, Y.; Zheng, Y.; He, F.; Yu, Z.; Huang, J.; Wang, H.; Ok, Y. S.; Jiang, Y.; Gao, B. Surface functional groups of carbon-based adsorbents and their roles in the removal of heavy metals from aqueous solutions: A critical review. *Chem. Eng. J.* **2019**, *366*, 608−621.

(13) Shen, Z.; Zhang, Y.; Jin, F.; McMillan, O.; Al-Tabbaa, A. Qualitative and quantitative characterisation of adsorption mechanisms of lead on four biochars. *Sci. Total Environ.* **2017**, *609*, 1401−1410.

(14) Shen, Z.; Jin, F.; Wang, F.; McMillan, O.; Al-Tabbaa, A. Sorption of lead by Salisbury biochar produced from British broadleaf hardwood. *Bioresour. Technol.* **2015**, *193*, 553−556.

(15) Pan, L.; Nishimura, Y.; Takaesu, H.; Matsui, Y.; Matsushita, T.; Shirasaki, N. Effects of decreasing activated carbon particle diameter from 30 mu m to 140 nm on equilibrium adsorption capacity. *Water Res.* **2017**, *124*, 425−434.

(16) Park, J.-H.; Ok, Y. S.; Kim, S.-H.; Cho, J.-S.; Heo, J.-S.; Delaune, R. D.; Seo, D.-C. Competitive adsorption of heavy metals onto sesame straw biochar in aqueous solutions. *Chemosphere* **2016**, *142*, 77−83.

(17) Harter, R. D. Competitive Sorption of Cobalt, Copper, and Nickel Ions by a Calcium-Saturated Soil. *Soil Sci. Soc. Am. J.* **1992**, *56*, 444−449.

(18) Depci, T.; Kul, A. R.; Önal, Y. Competitive adsorption of lead and zinc from aqueous solution on activated carbon prepared from Van apple pulp: Study in single- and multi-solute systems. *Chem. Eng. J.* **2012**, *200−202*, 224−236.

(19) Boudrahem, F.; Aissani-Benissad, F.; Aït-Amar, H. Batch sorption dynamics and equilibrium for the removal of lead ions from aqueous phase using activated carbon developed from coffee residue activated with zinc chloride. *J. Environ. Manage.* **2009**, *90*, 3031−3039.

(20) Raji, F.; Saraeian, A.; Pakizeh, M.; Attarzadeh, F. Removal of Pb(II) from aqueous solution by mesoporous silica MCM-41 modified by ZnCl2: kinetics, thermodynamics, and isotherms. *RSC Adv.* **2015**, *5*, 37066−37077.

(21) Danish, M.; Hashim, R.; Rafatullah, M.; Sulaiman, O.; Ahmad, A.; Govind. Adsorption of Pb(II) Ions from Aqueous Solutions by Date Bead Carbon Activated with ZnCl2. *Clean* **2011**, *39*, 392−399.

(22) Mohammadi, S. Z.; Hamidian, H.; Moeinadini, Z. High surface area-activated carbon from Glycyrrhiza glabra residue by ZnCl2 activation for removal of Pb(II) and Ni(II) from water samples. *J. Ind. Eng. Chem.* **2014**, *20*, 4112−4118.

(23) Islam, M. S.; Kwak, J.-H.; Nzediegwu, C.; Wang, S.; Palansuriya, K.; Kwon, E. E.; Naeth, M. A.; El-Din, M. G.; Ok, Y. S.; Chang, S. X. Biochar heavy metal removal in aqueous solution depends on feedstock type and pyrolysis purging gas. *Environ. Pollut.* **2021**, *281*, 117094.

(24) Park, J.-H.; Wang, J. J.; Zhou, B.; Mikhael, J. E. R.; DeLaune, R. D. Removing mercury from aqueous solution using sulfurized biochar and associated mechanisms. *Environ. Pollut.* **2019**, *244*, 627−635.

(25) Li, Z.; Su, M.; Duan, X.; Tian, D.; Yang, M.; Guo, J.; Wang, S.; Hu, S. Induced biotransformation of lead (II) by Enterobacter sp in SO4-PO4-Cl-Para solution. *J. Hazard. Mater.* **2018**, *357*, 491−497.

(26) Mohan, D.; Kumar, H.; Sarswat, A.; Alexandre-Franco, M.; Pittman, C. U. Cadmium and lead remediation using magnetic oak

wood and oak bark fast pyrolysis bio-chars. *Chem. Eng. J.* **2014**, *236*, 513−528.
(27) Chen, H.; Zhang, J.; Tang, L.; Su, M.; Tian, D.; Zhang, L.; Li, Z.; Hu, S. Enhanced Pb immobilization via the combination of biochar and phosphate solubilizing bacteria. *Environ. Int.* **2019**, *127*, 395−401.
(28) Cao, X.; Ma, L. Q.; Singh, S. P.; Zhou, Q. Phosphate-induced lead immobilization from different lead minerals in soils under varying pH conditions. *Environ. Pollut.* **2008**, *152*, 184−192.
(29) Zhu, Y.; Zhu, Z. Q.; Zhao, X.; Liang, Y. P.; Huang, Y. H. Characterization, Dissolution, and Solubility of Lead Hydroxypyromorphite [Pb-5(PO4)(3)OH] at 25-45 °C. *J. Chem.* **2015**, *2015*, 269387.
(30) Zheng, R.-L.; Cai, C.; Liang, J.-H.; Huang, Q.; Chen, Z.; Huang, Y.-Z.; Arp, H. P. H.; Sun, G.-X. The effects of biochars from rice residue on the formation of iron plaque and the accumulation of Cd, Zn, Pb, As in rice (Oryza sativa L.) seedlings. *Chemosphere* **2012**, *89*, 856−862.
(31) Lu, K.; Yang, X.; Shen, J.; Robinson, B.; Huang, H.; Liu, D.; Bolan, N.; Pei, J.; Wang, H. Effect of bamboo and rice straw biochars on the bioavailability of Cd, Cu, Pb and Zn to Sedum plumbizincicola. *Agric. Ecosyst. Environ.* **2014**, *191*, 124−132.
(32) Zheng, R.; Li, C.; Sun, G.; Xie, Z.; Chen, J.; Wu, J.; Wang, Q. The influence of particle size and feedstock of biochar on the accumulation of Cd, Zn, Pb, and As by Brassica chinensis L. *Environ. Sci. Pollut. Res.* **2017**, *24*, 22340−22352.
(33) Fahmi, A. H.; Samsuri, A. W.; Jol, H.; Singh, D. Physical modification of biochar to expose the inner pores and their functional groups to enhance lead adsorption. *RSC Adv.* **2018**, *8*, 38270−38280.
(34) Son, E.-B.; Poo, K.-M.; Mohamed, H. O.; Choi, Y.-J.; Cho, W.-C.; Chae, K.-J. A novel approach to developing a reusable marine macro-algae adsorbent with chitosan and ferric oxide for simultaneous efficient heavy metal removal and easy magnetic separation. *Bioresour. Technol.* **2018**, *259*, 381−387.
(35) Zhang, W.; Du, W.; Wang, F.; Xu, H.; Zhao, T.; Zhang, H.; Ding, Y.; Zhu, W. Comparative study on Pb2+ removal from aqueous solutions using biochars derived from cow manure and its vermicompost. *Sci. Total Environ.* **2020**, *716*, 137108.
(36) Matsui, Y.; Sakamoto, A.; Nakao, S.; Taniguchi, T.; Matsushita, T.; Shirasaki, N.; Sakamoto, N.; Yurimoto, H. Isotope Microscopy Visualization of the Adsorption Profile of 2-Methylisoborneol and Geosmin in Powdered Activated Carbon. *Environ. Sci. Technol.* **2014**, *48*, 10897−10903.
(37) Li, Z.; Su, M.; Tian, D.; Tang, L.; Zhang, L.; Zheng, Y.; Hu, S. Effects of elevated atmospheric CO2 on dissolution of geological fluorapatite in water and soil. *Sci. Total Environ.* **2017**, *599−600*, 1382−1387.
(38) Chen, H.; Ma, J.; Wei, J.; Gong, X.; Yu, X.; Guo, H.; Zhao, Y. Biochar increases plant growth and alters microbial communities via regulating the moisture and temperature of green roof substrates. *Sci. Total Environ.* **2018**, *635*, 333−342.
(39) Chen, H.; Tang, L.; Wang, Z.; Su, M.; Tian, D.; Zhang, L.; Li, Z. Evaluating the protection of bacteria from extreme Cd (II) stress by P-enriched biochar. *Environ. Pollut.* **2020**, *263*, 114483.
(40) Malash, G. F.; El-Khaiary, M. I. Piecewise linear regression: A statistical method for the analysis of experimental adsorption data by the intraparticle-diffusion models. *Chem. Eng. J.* **2010**, *163*, 256−263.
(41) Shen, Z.; Zhang, Y.; McMillan, O.; Jin, F.; Al-Tabbaa, A. Characteristics and mechanisms of nickel adsorption on biochars produced from wheat straw pellets and rice husk. *Environ. Sci. Pollut. Res.* **2017**, *24*, 12809−12819.

https://doi.org/10.1021/acsomega.1c04901
ACS Omega 2022, 7, 496−503